Global Biogeochemical Cycles

RESEARCH ARTICLE
10.1002/2017GB005809

An Analytical Framework for the Steady State Impact of Carbonate Compensation on Atmospheric CO_2

Anne Willem Omta[1], **Raffaele Ferrari**[1], **and David McGee**[1]

[1]Department of Earth, Atmospheric and Planetary Sciences, Massachusetts Institute of Technology, Cambridge, MA, USA

Key Points:
- We formulate an analytical model for the ocean carbon cycle on multimillennial timescales
- Carbonate compensation amplifies by 15% changes in atmospheric CO_2 due to changes in ocean temperature, salinity, or nutrient utilization
- Organic matter burial in the ocean, in combination with carbonate compensation, leads to outgassing of CO_2 from the ocean to the atmosphere

Correspondence to:
A. W. Omta,
omta@mit.edu

Citation:
Omta, A. W., Ferrari, R., & McGee, D. (2018). An analytical framework for the steady state impact of carbonate compensation on atmospheric CO_2. *Global Biogeochemical Cycles*, *32*, 720–735. https://doi.org/10.1002/2017GB005809

Received 6 OCT 2017
Accepted 19 MAR 2018
Accepted article online 27 MAR 2018
Published online 26 APR 2018

Abstract The deep-ocean carbonate ion concentration impacts the fraction of the marine calcium carbonate production that is buried in sediments. This gives rise to the carbonate compensation feedback, which is thought to restore the deep-ocean carbonate ion concentration on multimillennial timescales. We formulate an analytical framework to investigate the impact of carbonate compensation under various changes in the carbon cycle relevant for anthropogenic change and glacial cycles. Using this framework, we show that carbonate compensation amplifies by 15–20% changes in atmospheric CO_2 resulting from a redistribution of carbon between the atmosphere and ocean (e.g., due to changes in temperature, salinity, or nutrient utilization). A counterintuitive result emerges when the impact of organic matter burial in the ocean is examined. The organic matter burial first leads to a slight decrease in atmospheric CO_2 and an increase in the deep-ocean carbonate ion concentration. Subsequently, enhanced calcium carbonate burial leads to outgassing of carbon from the ocean to the atmosphere, which is quantified by our framework. Results from simulations with a multibox model including the minor acids and bases important for the ocean-atmosphere exchange of carbon are consistent with our analytical predictions. We discuss the potential role of carbonate compensation in glacial-interglacial cycles as an example of how our theoretical framework may be applied.

1. Introduction

The partitioning of carbon between the ocean and the atmosphere is key for understanding glacial-interglacial changes in atmospheric CO_2 (Archer et al., 2000; Menviel et al., 2008; Omta et al., 2006), as well as for predicting the fate of anthropogenic CO_2 (Archer, 2005; Archer et al., 2009; Montenegro et al., 2007). By combining carbon mass balances with carbonate chemistry, analytical expressions have been derived to describe the ocean-atmosphere partitioning of carbon on multicentennial to millennial timescales (d'Orgeville et al., 2011; Goodwin et al., 2007, 2008, 2009; Ito & Follows, 2005; Kwon et al., 2011; Marinov, Follows, et al., 2008; Marinov, Gnanadesikan, et al., 2008; Omta et al., 2010, 2011). In our view, the great benefit of this analytical approach is that it leads to a quantitative intuition for the system. With such a quantitative intuition, it is easier to assess which mechanisms have the largest impact on the atmospheric and oceanic carbon budgets, before embarking on time-consuming simulations. Here we apply the analytical approach to mechanisms repartitioning carbon between the ocean and the atmosphere on multimillennial timescales.

On multimillennial timescales, the ocean-atmosphere partitioning of carbon interacts with the ocean alkalinity cycle. Essentially, ocean alkalinity is the concentration of bases (e.g., CO_3^{2-}) available to react with CO_2 to form HCO_3^-. Alkalinity is transported into the ocean as a consequence of continental rock weathering and removed from the ocean through sedimentation and burial of calcifying organisms (see Figure 1). It is generally assumed that the ocean maintains a balance between these input and output fluxes of alkalinity through a mechanism referred to as carbonate compensation, which works as follows. The CO_3^{2-} concentration ($[CO_3^{2-}]$) is lower in the deep ocean than at the surface, mainly because the soft-tissue carbon pump transfers carbon from the upper to the deep ocean (Volk & Hoffert, 1985). Furthermore, the solubility of calcium carbonate ($CaCO_3$) increases with pressure (Pytkowicz & Conners, 1964). Due to a combination of these effects, much of the deep ocean is undersaturated with respect to calcite (Ridgwell & Zeebe, 2005). At a level named the carbonate compensation depth (CCD), the rates of sedimentation and dissolution of calcite are equal. Below this level, there is no $CaCO_3$ present in sediments. A decrease of the deep-ocean $[CO_3^{2-}]$ leads to an increase in both the dissolution of $CaCO_3$ from sediments and a decrease in the accumulation of new $CaCO_3$ sediments.

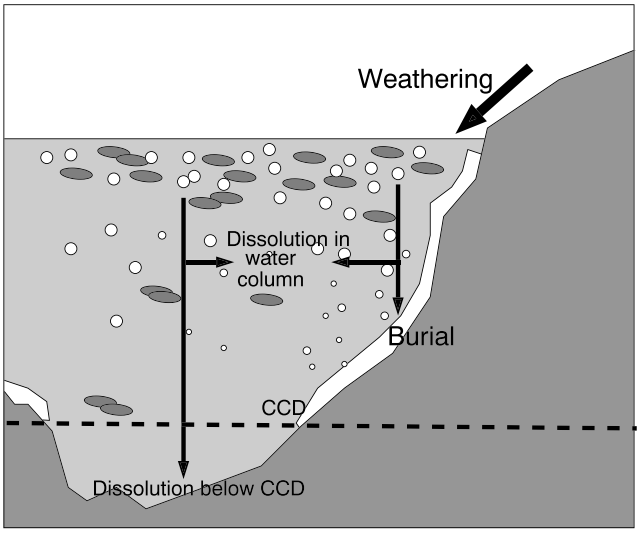

Figure 1. A schematic depiction of the input and output of alkalinity into and out of the ocean (figure adapted from Omta et al., 2013). Alkalinity is added to the ocean through river runoff and is consumed by calcifiers and removed from the ocean through calcifier sedimentation. Above the carbonate compensation depth (CCD), calcium carbonate accumulates, whereas it dissolves below the CCD. A decrease in deep-ocean $[CO_3^{2-}]$ leads to a decrease in $CaCO_3$ output and, thus, an increase in deep-ocean $[CO_3^{2-}]$. This carbonate compensation feedback is thought to return the deep-ocean $[CO_3^{2-}]$ to its equilibrium value on a multimillennial timescale.

This, in turn, leads to an increase in the deep-ocean $[CO_3^{2-}]$. Overall, the deep-ocean $[CO_3^{2-}]$ is expected to relax back to its original value, as long as the alkalinity input into the ocean by, for example, rivers does not change (Archer & Maier-Reimer, 1994; Sigman et al., 1998). The increased sediment dissolution and the decreased sediment accumulation mechanisms occur on two different timescales (Archer et al., 1997, 1998; Ridgwell & Hargreaves, 2007). Based on a suite of carbon release experiments with the carbon-centric Grid ENabled Integrated Earth system model (cGENIE), Lord et al. (2016) combined these two timescales into a single response time of 4–16 kyr (depending on the total carbon emissions). However, as a result of continuous equilibration and reequilibration of carbon between the atmosphere, ocean, and sediments, the overall relaxation has a long tail stretching tens of thousands of years.

Running numerical simulations for tens of thousands of years until full carbonate compensation has been achieved is very time consuming. Thus, simple analytical expressions for estimating the impact of carbonate compensation on atmospheric CO_2 are very useful, particularly if various different disturbances are to be investigated. Using the argument that $[CO_3^{2-}]$ returns to its original value, Goodwin and Ridgwell (2010) derived such an expression for the ocean-atmosphere partitioning of anthropogenic carbon on multimillennial timescales. From this expression, Goodwin and Ridgwell (2010) estimated that between 6% and 10% of anthropogenic carbon will remain in the atmosphere after carbonate compensation has been completed. We extend their work by deriving analytical expressions to estimate the overall impact of carbonate compensation in response to variations in ocean temperature, salinity, and nutrient utilization and the total ocean nutrient inventory (section 2). We compare the main predictions from our analytical framework against simulations with a multibox model including the full set of compounds involved in the ocean-atmosphere exchange of carbon, which is described in detail in Appendix A. We believe that the expressions derived here will be useful both for understanding how future climate change may feed back onto the marine carbon cycle and for understanding glacial-interglacial CO_2 changes. We provide a more detailed discussion of the potential relevance of our findings for the future and the past carbon cycle in sections 3 and 4.

2. Analytical Framework

We start from a balance equation for carbon in the ocean-atmosphere system (Ito & Follows, 2005; Williams & Follows, 2011):

$$MX_{CO_2} + V\left(C_{sat} + C_{reg} + C_{carb}\right) = I_{oa} \quad (1)$$

with M the total gas content of the atmosphere (mol), V the volume of the ocean (m^3), X_{CO_2} the atmospheric CO_2 mixing ratio (ppmv), and I_{oa} the total carbon inventory of the ocean-atmosphere system (mol). C_{sat}, C_{reg}, and C_{carb} (all in mol/m^3) describe the partitioning of dissolved inorganic carbon (DIC) into the different carbon pumps introduced by Volk and Hoffert (1985). C_{sat} is the average oceanic saturated carbon concentration, which is somewhat higher than the average saturated carbon concentration at the ocean surface as a result of the lower temperature of the deep ocean (the solubility pump), C_{reg} is the average regenerated carbon concentration (the soft-tissue pump), and C_{carb} is the carbon added to the ocean through dissolution of sinking $CaCO_3$ (the carbonate pump).

The process of carbonate compensation leads to a change in the total carbon inventory of the ocean-atmosphere system because of the dissolution and burial of $CaCO_3$. We will refer to such changes in I_{oa} as $\delta I_{oa,calc}$. Furthermore, carbon can be added or removed from the ocean-atmosphere system in forms other than $CaCO_3$, for example, through anthropogenic carbon emissions and burial of particulate organic carbon (POC). We will refer to such changes in I_{oa} as $\delta I_{oa,noncalc}$. Equation (1) can be used to relate the changes in the total carbon inventory to changes in X_{CO_2}, C_{sat}, C_{reg}, and C_{carb}:

$$M\delta X_{CO_2} + V\delta\left(C_{sat} + C_{reg} + C_{carb}\right) = \delta I_{oa,calc} + \delta I_{oa,noncalc} \tag{2}$$

For every mole of carbon in $CaCO_3$ that is added, the ocean gains two moles of alkalinity. Thus, $\delta I_{oa,calc} = \frac{V\delta A}{2}$, with A the alkalinity. Furthermore, if we neglect the contributions to alkalinity from all acids and bases other than HCO_3^- and CO_3^{2-}, then $\delta A \approx \delta[HCO_3^-]+2\delta[CO_3^{2-}]$. Neglecting dissolved CO_2, $\delta\left(C_{sat} + C_{reg} + C_{carb}\right) \approx \delta[HCO_3^-]+\delta[CO_3^{2-}]$. Hence, $\delta A \approx \delta\left(C_{sat} + C_{reg} + C_{carb}\right) + \delta[CO_3^{2-}]$.

Following earlier analytical work on the impact of carbonate compensation (Goodwin & Ridgwell, 2010), the difference between the whole-ocean and deep-ocean average $[CO_3^{2-}]$ is neglected. The underlying assumption is that DIC and alkalinity are vertically homogeneous throughout most of the ocean. This seems a reasonable approximation for the current ocean, in which vertical gradients in DIC and alkalinity are rather small below ~1,000 m (Chester, 2000). With this assumption (discussed in more detail in section 3.1), we can equate the whole-ocean average $[CO_3^{2-}]$ to the $[CO_3^{2-}]$ at the CCD, relevant for carbonate compensation. Thus, we state that $\delta[CO_3^{2-}] = 0$ after full carbonate compensation, which means that $\delta A \approx \delta\left(C_{sat} + C_{reg} + C_{carb}\right)$. Altogether, this gives

$$M\delta X_{CO_2} + \frac{V\delta\left(C_{sat} + C_{reg} + C_{carb}\right)}{2} = \delta I_{oa,noncalc} \tag{3}$$

Essentially, the term $V\delta\left(C_{sat} + C_{reg} + C_{carb}\right)$ in equation (1) has been replaced in equation (3) by a term $\frac{V\delta\left(C_{sat}+C_{reg}+C_{carb}\right)}{2}$. The factor $\frac{1}{2}$ expresses that any transfer of carbon between the atmosphere and ocean will account for the full change in atmospheric carbon but only half of the change in oceanic carbon. This reflects the very nature of the carbonate compensation process: for every CO_2 molecule that the ocean takes up, the ocean also needs to take up a CO_3^{2-} ion from the sediment to restore the original $[CO_3^{2-}]$. This is an approximation, because CO_3^{2-} and CO_2 also react with minor acids and bases, such as the boron species, H^+, and OH^-. However, it appears to be sufficiently accurate for our purposes, as we demonstrate in sections 2.1 and 2.2 through comparisons between our analytical predictions and simulations with a multibox model that includes these minor acids and bases.

In section 2.1, we derive an expression for the change in atmospheric CO_2, if carbon is redistributed within the ocean-atmosphere system. In other words, we assume: $\delta I_{oa,noncalc} = 0$. Such a carbon redistribution could be due to a change in ocean temperature or salinity or a change in nutrient utilization. Without carbonate compensation, there would be no change in the total ocean-atmosphere carbon inventory, but the carbonate compensation process leads to input or output of carbon in the form of $CaCO_3$. In section 2.2, we derive an expression for the change in atmospheric CO_2, if some POC is buried instead of being remineralized in the water column. In other words: $\delta I_{oa,noncalc} = \delta I_{oa,bur}$. To maintain deep-ocean $[CO_3^{2-}]$ at its original value, C_{reg} and $CaCO_3$ need to be removed in a 1:1 ratio. The resulting alkalinity decrease then leads to outgassing of CO_2 from the ocean to the atmosphere.

2.1. Carbonate Compensation in Response to Redistribution of Carbon in the Ocean-Atmosphere System

If the only changes in the total carbon inventory in the ocean-atmosphere system are due to the carbonate compensation process, then equation (3) becomes

$$M\delta X_{CO_2} + \frac{V\delta\left(C_{sat} + C_{reg} + C_{carb}\right)}{2} = 0 \tag{4}$$

The saturated carbon concentration is determined by the atmospheric CO_2 content and by the ocean temperature, salinity, and alkalinity. As in Goodwin and Lenton (2009), we split the dependencies of C_{sat} into contributions from atmospheric CO_2, temperature, alkalinity, and salinity, with $B \equiv \frac{\partial lnX_{CO_2}}{\partial lnC_{sat}}$ the Revelle buffer factor (Bolin & Eriksson, 1959), $\gamma_T \equiv \frac{\partial C_{sat}}{\partial T}$, $\gamma_S \equiv \frac{\partial C_{sat}}{\partial S}$, and $\gamma_A \equiv \frac{\partial C_{sat}}{\partial A}$. The change in ocean alkalinity (δA) is divided into a change in preformed alkalinity (δA_{pref}), relevant for the ocean-atmosphere carbon partitioning, a change due to the carbonate pump ($\delta A_{carb} = 2\delta C_{carb}$) and a change due to the remineralization of organic matter (Sarmiento & Gruber, 2006) ($\delta A_{reg} = -R_{N:C}\delta C_{reg}$, with $R_{N:C}$ the Redfield N:C ratio). The expansion of δC_{sat} gives

$$\begin{aligned}\delta C_{sat} &= \frac{C_{sat}}{X_{CO_2}B}\delta X_{CO_2} + \gamma_T\delta T + \gamma_S\delta S + \gamma_A\delta A_{pref}\\ &= \frac{C_{sat}}{X_{CO_2}B}\delta X_{CO_2} + \gamma_T\delta T + \gamma_S\delta S + \gamma_A\delta\left(A - A_{carb} - A_{reg}\right)\\ &= \frac{C_{sat}}{X_{CO_2}B}\delta X_{CO_2} + \gamma_T\delta T + \gamma_S\delta S + \gamma_A\delta\left(C_{sat} + C_{reg} + C_{carb}\right)\\ &\quad + \gamma_A\left(R_{N:C}\delta C_{reg} - 2\delta C_{carb}\right)\end{aligned} \tag{5}$$

which can be rearranged thus:

$$\delta\left(C_{sat} + C_{reg} + C_{carb}\right) = \frac{\frac{C_{sat}}{X_{CO_2}B}\delta X_{CO_2} + \gamma_T\delta T + \gamma_S\delta S + \left(1 + R_{N:C}\right)\delta C_{reg} - \left(2\gamma_A - 1\right)\delta C_{carb}}{1 - \gamma_A} \tag{6}$$

Substituting equation (6) into (4), we obtain

$$\left(1 - \gamma_A\right)M\delta X_{CO_2} = -\frac{V}{2}\left(\frac{C_{sat}}{X_{CO_2}B}\delta X_{CO_2} + \gamma_T\delta T + \gamma_S\delta S + \left(1 + R_{N:C}\right)\delta C_{reg} - (2\gamma_A - 1)\delta C_{carb}\right) \tag{7}$$

which can be used to calculate the change in atmospheric X_{CO_2}:

$$\delta X_{CO_2} = -\frac{\gamma_T\delta T + \gamma_S\delta S + \left(1 + R_{N:C}\right)\delta C_{reg} - \left(2\gamma_A - 1\right)\delta C_{carb}}{2\left(1 - \gamma_A\right)\frac{M}{V} + \frac{C_{sat}}{X_{CO_2}B}} \tag{8}$$

This is the change in atmospheric X_{CO_2} after carbonate compensation resulting from a change in ocean temperature (δT), salinity (δS), nutrient utilization (δC_{reg}), or the carbonate pump (δC_{carb}). Combining equation (8) with the balance equation (4) and $\delta A \approx \delta\left(C_{sat} + C_{reg} + C_{carb}\right)$, the result can also be expressed in terms of whole-ocean alkalinity:

$$\delta A = -\frac{2M\delta X_{CO_2}}{V} = \frac{\gamma_T\delta T + \gamma_S\delta S + \left(1 + R_{N:C}\right)\delta C_{reg} - \left(2\gamma_A - 1\right)\delta C_{carb}}{1 - \gamma_A + \frac{C_{sat}}{X_{CO_2}B}\frac{V}{2M}} \tag{9}$$

Without carbonate compensation, the change in X_{CO_2} would be

$$\delta X_{CO_2} = -\frac{\gamma_T\delta T + \gamma_S\delta S + \left(1 + R_{N:C}\right)\delta C_{reg} - \left(2\gamma_A - 1\right)\delta C_{carb}}{\frac{M}{V} + \frac{C_{sat}}{X_{CO_2}B}} \tag{10}$$

which is essentially a restatement of results derived in various earlier papers (Goodwin et al., 2008, 2011; Marinov, Follows, et al., 2008; Marinov, Gnanadesikan, et al., 2008; Omta et al., 2011).

The ratio of δX_{CO_2} with carbonate compensation to δX_{CO_2} without carbonate compensation is thus

$$\frac{\delta X_{CO_2}(carbocomp.)}{\delta X_{CO_2}(nocarbocomp.)} = \frac{MX_{CO_2} + \frac{VC_{sat}}{B}}{2\left(1-\gamma_A\right)MX_{CO_2} + \frac{VC_{sat}}{B}} \tag{11}$$

Using $M = 1.80\times10^{20}$ mol, $X_{CO_2} = 300$ ppmv, $V = 1.40\times10^{18}$ m^3, $\gamma_A = 0.90$, $C_{sat} = 2.00$ mol/m^3, and $B = 12.0$, we get

$$\frac{\delta X_{CO_2}(carbocomp.)}{\delta X_{CO_2}(nocarbocomp.)} \approx 1.18 \tag{12}$$

That is, carbonate compensation enhances the change in atmospheric CO_2 by about 18% after a redistribution of carbon between the atmosphere and the ocean. This value must have varied in the geological past, in particular because there have been variations in X_{CO_2}.

To test this prediction of an ~18% enhancement of CO_2 changes against more precise calculations including the minor acids and bases important for the ocean-atmosphere exchange of carbon (the boron species, H^+, and OH^-), we use the multibox model described in Appendix A. The response of the ocean-atmosphere carbon partitioning to a perturbation in ocean temperature, salinity, or carbon pumps is expected to occur on three timescales (Lord et al., 2016): (1) a multicentennial equilibration of carbon between the atmosphere and ocean, without significant interaction with the sediments; (2) a multimillennial equilibration with the calcite sediments through the carbonate compensation feedback; and (3) a final equilibration of the ocean alkalinity cycle due to adjustments in the silicate weathering rate on timescales of many hundreds of thousands of years.

In the simulations, we study the X_{CO_2} response to perturbations in the ocean on the first two of these timescales, neglecting long-term changes in the silicate weathering rate. First, we let the box model equilibrate on the faster timescale without carbonate compensation, after which we turn on the carbonate compensation to study the slower equilibration through the carbonate compensation feedback. In our multibox model, the carbonate compensation process is formulated as a linear relaxation toward an equilibrium deep-ocean $[CO_3^{2-}]$ with a 5 kyr time constant.

The model is spun up for 200 kyr to equilibration with carbonate compensation switched on. With the imposed equilibrium deep-ocean $[CO_3^{2-}]$, ocean temperatures, and carbon and phosphorus inventories, the steady state X_{CO_2} settles at 297 ppmv. Subsequently, we run a set of experiments in which the temperature of all the ocean surface boxes is changed, with and without carbonate compensation. As expected, a temperature change has a somewhat stronger impact on atmospheric CO_2 with carbonate compensation than without it (Figure 2). The ratio $\frac{\delta X_{CO_2}(carbocomp.)}{\delta X_{CO_2}(nocarbocomp.)}$ increases from 1.15 to 1.21, as the imposed temperature change increases from −5 to +5 °C (Figure 2b), which can be understood as follows. Since $2(1-\gamma_A)$ is only about 0.2, equation (11) can be approximated as $\frac{\delta X_{CO_2}(carbocomp.)}{\delta X_{CO_2}(nocarbocomp.)} \approx \frac{MX_{CO_2}B}{VC_{sat}} + 1$. As X_{CO_2} increases with increasing temperature, $\frac{VC_{sat}}{B}$ remains relatively constant, which leads to the overall increase in the ratio.

To give an idea of the transient dynamics with and without carbonate compensation, we show full time series of X_{CO_2}, as well as DIC and alkalinity in the Antarctic Bottom Water (AABW) box. First, the sea surface temperatures (SST) are decreased by 5 °C without carbonate compensation (Figure 3). The temperature change leads to a repartitioning of carbon between the atmosphere and the ocean: X_{CO_2} decreases by 48 ppmv (green line in Figure 3a), while DIC increases by 7 μM (green line in Figure 3b). The alkalinity remains constant, as long as there is no carbonate compensation (green line in Figure 3c). After 10 kyr, the system has equilibrated and we switch the carbonate compensation on, while the low SST are maintained. The carbonate compensation process leads to a further decrease in atmospheric X_{CO_2} of just over 7 ppmv (blue line in Figure 3a), an increase in DIC of 9 μM (blue line in Figure 3b), and an increase in alkalinity of 16 μM (blue line in Figure 3c). This is slightly more than the alkalinity change expected from our framework: $\delta A = -\frac{2M\delta X_{CO_2}}{V}$=14 μM, which is likely due to the contributions from minor acids and bases such as the boron species. The carbonate compensation takes place on a timescale much longer than the imposed 5 kyr response time because of the asymptotic nature of the overall equilibration process. That is, a certain change in temperature leads to a certain change

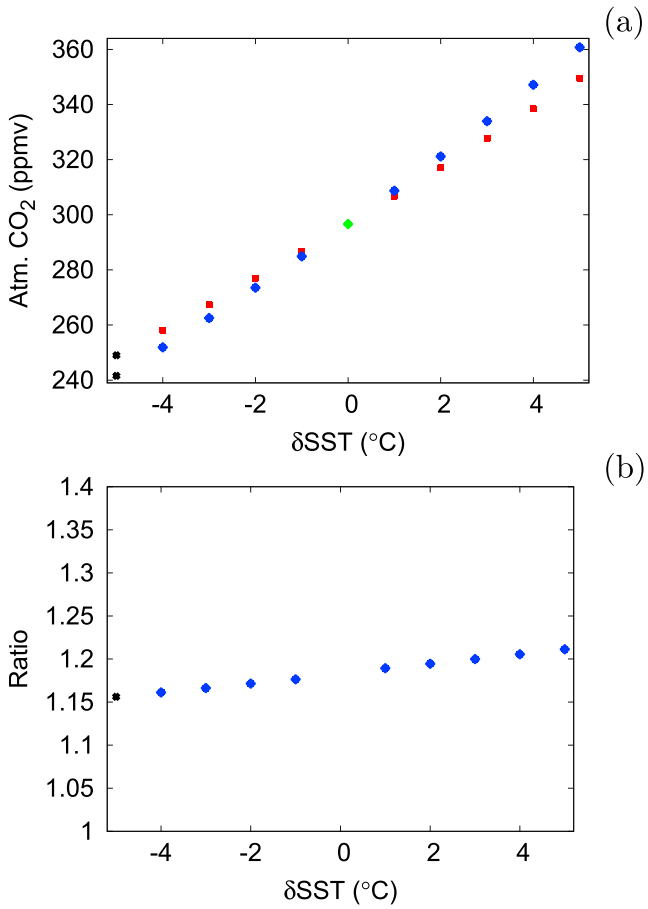

Figure 2. (a) Atmospheric CO_2 as a function of the change in global mean sea surface temperature (SST), after a 250 kyr equilibration with carbonate compensation (blue diamonds) and without carbonate compensation (red squares). The green diamond indicates the spin-up simulation; the black crosses indicate the simulation experiment shown in Figure 3. (b) The ratio $\frac{\delta X_{CO_2}(carbocomp.)}{\delta X_{CO_2}(nocarbocomp.)}$ as a function of the change in global mean SST; again, the black cross indicates the simulation experiment shown in Figure 3.

in X_{CO_2} and deep-ocean DIC. This leads to $CaCO_3$ dissolution or burial, which in turn leads to a change in atmospheric X_{CO_2}, which in turn leads to $CaCO_3$ dissolution or burial, which in turn leads to a change in atmospheric X_{CO_2}, etc.

2.2. Carbonate Compensation in Response to Organic Matter Burial

If organic carbon and phosphorus are buried instead of being remineralized, then there is a decrease in the inventory of regenerated carbon equal to the decrease in the total carbon inventory: $\delta I_{oa,noncalc} = \delta I_{oa,bur} = V\delta C_{reg}$. In this case, equation (3) becomes

$$M\delta X_{CO_2} + \frac{V\delta\left(C_{sat} + C_{reg} + C_{carb}\right)}{2} = V\delta C_{reg} \tag{13}$$

or

$$M\delta X_{CO_2} + \frac{V\delta\left(C_{sat} - C_{reg} + C_{carb}\right)}{2} = 0 \tag{14}$$

We use an expansion analogous to equation (5) but ignoring any changes in the temperature and salinity, because the focus is on changes in the nutrient inventory:

$$\begin{aligned}\delta\left(C_{sat} - C_{reg} + C_{carb}\right) &= \frac{C_{sat}}{X_{CO_2}B}\delta X_{CO_2} \\ &+ \gamma_A\delta\left(C_{sat} + C_{reg} + C_{carb}\right) + \gamma_A\left(R_{N:C}\delta C_{reg} - 2\delta C_{carb}\right) - \delta C_{reg} + \delta C_{carb}\end{aligned} \tag{15}$$

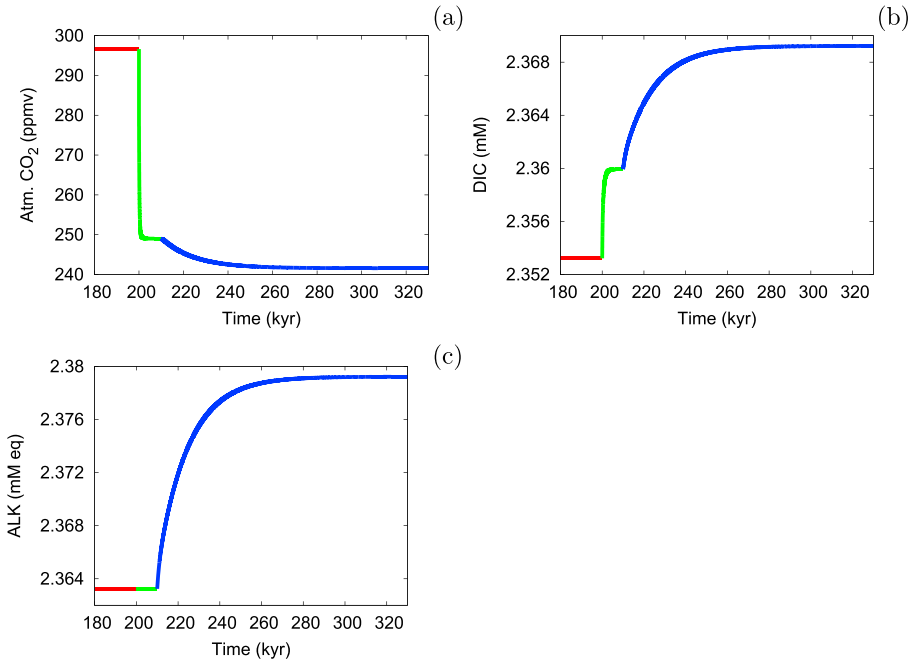

Figure 3. Multibox model simulation: after the spin-up (red line), the sea surface temperature is decreased by 5 °C everywhere, first without carbonate compensation (green line) and finally with carbonate compensation (blue line); (a) atmospheric CO_2, (b) dissolved inorganic carbon (DIC) in the Antarctic Bottom Water box, and (c) total alkalinity in the Antarctic Bottom Water box.

Collecting $\delta\left(C_{\text{sat}} - C_{\text{reg}} + C_{\text{carb}}\right)$ terms on the left-hand side and dividing by $1-\gamma_A$ gives

$$\delta\left(C_{\text{sat}} - C_{\text{reg}} + C_{\text{carb}}\right) = \frac{\frac{C_{\text{sat}}}{X_{CO_2} B}\delta X_{CO_2}\left(2\gamma_A - 1 + R_{N:C}\right)\delta C_{\text{reg}} - \left(2\gamma_A - 1\right)\delta C_{\text{carb}}}{1-\gamma_A} \tag{16}$$

Combining equations (14) and (16) then leads to

$$\delta X_{CO_2} = -\frac{\left(2\gamma_A - 1 + R_{N:C}\right)\delta C_{\text{reg}} - \left(2\gamma_A - 1\right)\delta C_{\text{carb}}}{2\left(1-\gamma_A\right)\frac{M}{V} + \frac{C_{\text{sat}}}{X_{CO_2} B}} \tag{17}$$

Equation (17), which describes the impact of burial of POC on δX_{CO_2}, is identical to equation (8), which applies to a change in nutrient utilization (setting δT and δS equal to 0), except that the factor $1+R_{N:C}$ in front of δC_{reg} is replaced by $2\gamma_A - 1 + R_{N:C}$. Given that $\frac{2\gamma_A - 1 + R_{N:C}}{1+R_{N:C}} \approx 0.8$, the change in atmospheric CO_2 after carbonate compensation is ~20% smaller if it is caused by POC burial than if it is caused by a decreased nutrient utilization, for a given decrease in the regenerated carbon δC_{reg}.

Using equation (13) and $\delta A \approx \delta\left(C_{\text{sat}} + C_{\text{reg}} + C_{\text{carb}}\right)$, equation (17) can also be cast as an expression for the whole-ocean alkalinity change:

$$\begin{aligned}\delta A &= 2\left(-\frac{M\delta X_{CO_2}}{V} + \delta C_{\text{reg}}\right) \\ &= \frac{\left(2\gamma_A - 1 + R_{N:C}\right)\delta C_{\text{reg}} - \left(2\gamma_A - 1\right)\delta C_{\text{carb}}}{1 - \gamma_A + \frac{C_{\text{sat}}}{X_{CO_2} B}\frac{V}{2M}} + 2\delta C_{\text{reg}}\end{aligned} \tag{18}$$

The sinkings of POC and $CaCO_3$ are intimately connected with each other (Klaas & Archer, 2002). Consistently, we assume that the whole-ocean average strengths of the carbonate pump and the soft-tissue pump

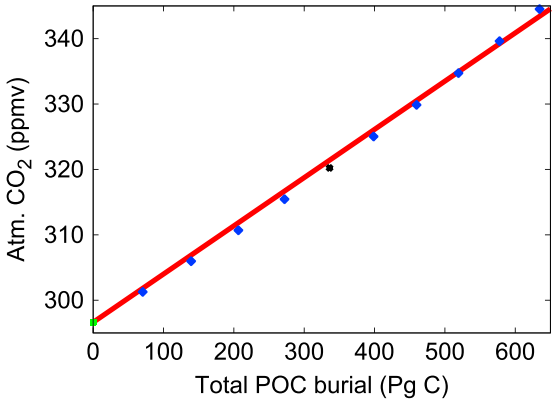

Figure 4. Atmospheric CO_2 as a function of the total amount of buried particulate organic carbon (POC), after a 250-kyr equilibration with carbonate compensation (blue diamonds). The green diamond indicates the spin-up simulation; the black cross stands for the simulation experiment shown in Figure 5. The red line indicates the slope predicted by relation (19), using $M = 1.80 \times 10^{20}$ mol, $X_{CO_2} = 300$ ppmv, $V = 1.40 \times 10^{18}$ m^3, $\gamma_A = 0.90$, $C_{sat} = 2.00$ mol/m^3, $B = 12.0$, and $R_{calc} = 0.100$. In calculating this slope, the alkalinity change directly resulting from the remineralization of organic matter ($\delta A_{reg} = -R_{N:C}\delta C_{reg}$) was neglected, because this effect is not included in our multibox model.

are proportional to each other: $C_{carb} = R_{calc}C_{reg}$ (with R_{calc} the whole-ocean average ratio of $CaCO_3$:organic carbon added to the water column). If using an average R_{calc} value for the whole ocean is a valid approximation, then equation (17) can be rewritten as

$$\delta X_{CO_2} = -\frac{\left((2\gamma_A - 1)(1 - R_{calc}) + R_{N:C}\right)\delta C_{reg}}{2\left(1 - \gamma_A\right)\frac{M}{V} + \frac{C_{sat}}{X_{CO_2}B}} \tag{19}$$

The ratio R_{calc} determines to what extent the carbonate compensation in the deep ocean is communicated to the ocean surface. If this ratio were 1:1, then the weakening of the soft-tissue carbon pump and the associated carbonate compensation would be offset exactly by a weakening of the carbonate pump, and $[CO_3^{2-}]$ at the ocean surface (and thus atmospheric CO_2) would remain constant. However, the average ratio of $CaCO_3$:POC added to the water column is believed to be in the 0.1–0.2:1 range (Boyle, 1988; Yamanaka & Tajika, 1996). Hence, a large fraction of the alkalinity output in the deep ocean is communicated to the surface ocean, because less carbon is added to the deep ocean through the carbonate pump than through the soft-tissue carbon pump.

To test equation (19), we again use our multibox model. In all the simulations, POC and organic phosphorus are exported from the surface in a fixed Redfield ratio of 106:1. After the 200-kyr spin-up during which all the exported POC and phosphorus are remineralized in the deep ocean, we switch on the burial. During 10 kyr, a fraction of the exported carbon and phosphorus is taken out of the ocean-atmosphere system in the 106:1 Redfield ratio instead of being remineralized, which reduces the strength of the soft-tissue carbon pump. Subsequently, the burial is switched

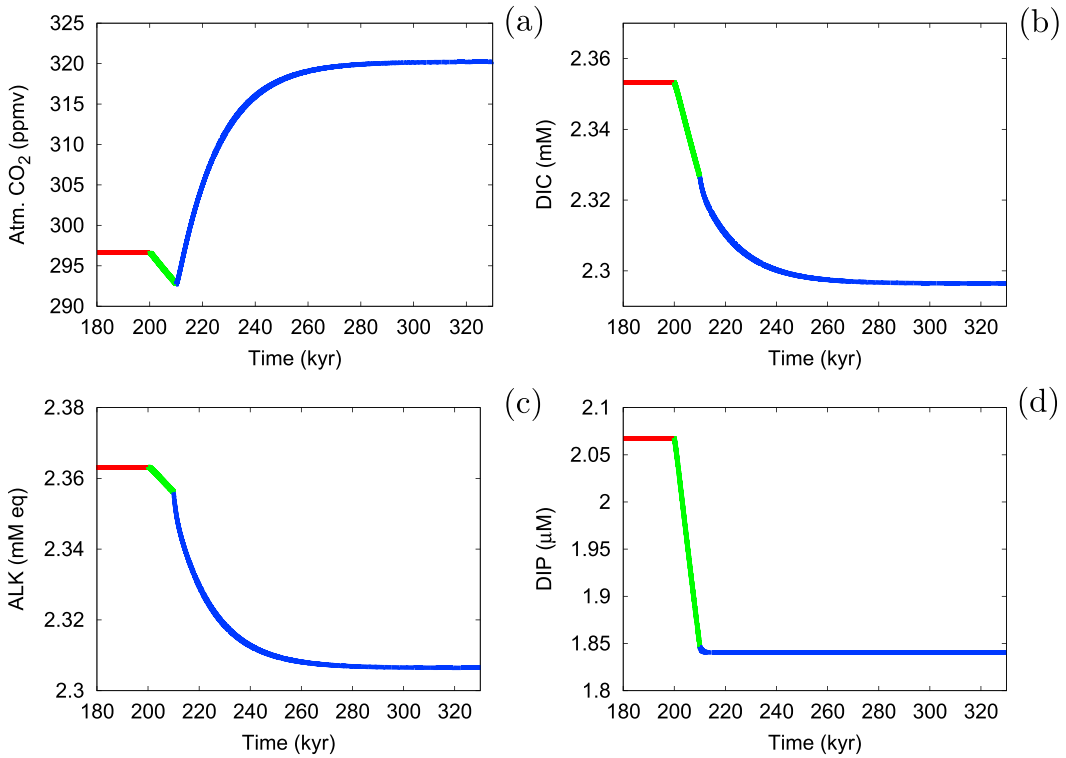

Figure 5. Multibox model simulation: after the spin-up (red line), organic carbon and phosphorus are buried (green line). Most of the carbonate compensation takes place after the burial has been halted (blue line). (a) Atmospheric CO_2, (b) dissolved inorganic carbon (DIC) in the Antarctic Bottom Water (AABW) box, (c) total alkalinity in the AABW box, and (d) dissolved inorganic phosphorus (DIP) in the AABW box.

off and the system is left to equilibrate. The carbonate compensation is switched on at all times. To vary the output of organic phosphorus and POC, we run a set of simulations where the burial fraction is increased from 0.2% to 2.0% in 0.2% increments. The total amount of phosphorus buried in the model experiments varied between 0.05×10^{15} and 0.50×10^{15} mol, out of a total initial inventory of 2.41×10^{15} mol; the total amount of POC buried varied between 70 Pg C and 630 Pg C. In Figure 4, we show atmospheric CO_2 as a function of the total amount of buried POC, after full equilibration (250 kyr) with carbonate compensation, along with the slope predicted by relation (19). As can be seen, there is excellent agreement between the analytical theory and the box model simulations.

In Figure 5, we show the time series of X_{CO_2}, as well as DIC, alkalinity, and dissolved inorganic phosphorus in the AABW box for one of the simulations. During the burial phase, there are two competing effects: the removal of phosphorus weakens the soft-tissue carbon pump and therefore increases atmospheric CO_2, whereas the removal of carbon decreases atmospheric CO_2. In our box model, the combined removal of carbon and phosphorus under the Redfield ratio before significant carbonate compensation leads to a minor decrease in X_{CO_2} (green line in Figure 5a). (This reflects that there is not full nutrient utilization. With full nutrient utilization across the ocean ($C_{reg} = R_{C:P}P$) and a removal of carbon and phosphorus according to the Redfield ratio ($\delta I_{oa,noncalc} = R_{C:P}\delta P$), then $I_{oa,noncalc} = \delta C_{reg}$. That is, equation (2) becomes: $M\delta X_{CO_2} + V\delta\left(C_{sat} + C_{carb}\right) = 0$. If C_{carb} does not change, then the net effect on atmospheric CO_2 is 0, as C_{sat} depends only on X_{CO_2}, temperature, salinity, and alkalinity.) During the burial phase, the major changes are in the ocean carbon and phosphorus inventories: DIC decreases by 27 μM (green line in Figure 5b), while the dissolved inorganic phosphorus concentration decreases by 0.22 μM (green line in Figure 5d). The alkalinity decrease is still relatively minor (green line in Figure 5c), because the carbonate compensation process responds to changes in the deep ocean $[CO_3^{2-}]$ with a lag of many thousands of years. After the burial phase, the carbonate compensation leads to a rather large increase in X_{CO_2} (blue line in Figure 5a), as well as major decreases in DIC and alkalinity (blue lines in Figures 5b/c), while the dissolved inorganic phosphorus concentration remains constant (blue line in Figure 5d). The overall increase in X_{CO_2} equals 24 ppmv, whereas the overall alkalinity decrease equals 57 μM eq. Based on $\delta A = 2\left(-\frac{M\delta X_{CO_2}}{V} + \delta C_{reg}\right)$, one would expect an alkalinity decrease of 61 μM eq, under the assumption that $\delta C_{reg} = R_{C:P}\delta P$. Again, the final state is only achieved after many tens of thousands of years, during which there is continuous equilibration and reequilibration between the different reservoirs.

3. Discussion

As in section 2, we first discuss carbonate compensation under a constant nutrient inventory (section 3.1), before moving to the potential combined impact of POC burial and carbonate compensation (section 3.2). Finally, we discuss how $CaCO_3$ preservation and production may impact the timescale at which deep-ocean $[CO_3^{2-}]$ is restored (section 3.3).

3.1. Constant Nutrient Inventory

Our analytical framework (as well as our multibox model) predicts that carbonate compensation increases by 15–20% the impact of changes in atmospheric CO_2 resulting from a redistribution of carbon between the atmosphere and ocean. The full changes in atmospheric CO_2 due to variations in the ocean temperature and the soft-tissue carbon pump can thus be inferred from coupled ocean-atmosphere-biogeochemistry models that do not include carbonate compensation and are therefore cheaper to run, because they equilibrate in multicentennial timescales rather than multimillennial timescales. The rule of thumb is then to multiply the model's predicted CO_2 changes by 1.15–1.20 to account for carbonate compensation.

The most important application of the 15–20% rule of thumb will likely be in the study of glacial-interglacial cycles. Ice core measurements suggest that atmospheric CO_2 dropped by 80–100 ppmv during glacial climates compared to interglacials (Lüthi et al., 2008; Petit et al., 1999). These drops may have involved various disturbances of the ocean carbon system (Chikamoto et al., 2012; Peacock et al., 2006; Wallmann, 2014), for example, changes in the whole-ocean temperature, salinity, alkalinity, and nutrient utilization. However, it remains unclear whether the net impact of all these ocean changes can amount to the total 80–100 ppmv swings in atmospheric CO_2 (Brovkin et al., 2012; Sigman & Boyle, 2000; Sigman et al., 2010). Our study suggests that changes in ocean temperature, salinity, alkalinity, and nutrient utilization need explain only 70–85 ppmv changes, because an additional 15–20% can be attributed to carbonate compensation.

Another important application of our result is to predict the long-term fate of anthropogenic carbon emissions, for which Goodwin and Ridgwell (2010) previously developed an analytical framework. They focused on the chemical processes (air-sea carbon partitioning and carbonate compensation) in isolation, without considering the impact of the changing climate on the ocean-atmosphere partitioning of CO_2. However, temperature is expected to change under global warming. Furthermore, it has been suggested that the soft-tissue carbon pump will strengthen in a high CO_2 world (Bernardello et al., 2014; Oschlies et al., 2008; Riebesell et al., 2007). All these hypothesized mechanisms essentially involve a redistribution of carbon between the ocean and the atmosphere, which means that their impacts on atmospheric CO_2 will be enhanced by 15–20% after carbonate compensation.

Our framework is built on an assumption that DIC and alkalinity are more or less vertically homogeneous throughout most of the ocean, which holds in the present-day ocean. The framework needs to be modified if there is a strong vertical heterogeneity in DIC at intermediate depths and in the abyss. In fact, this has already been demonstrated by earlier box model simulations (Hain et al., 2010). In these simulations, carbonate compensation enhanced the impact of changes in nutrient utilization on atmospheric CO_2 by 16% (i.e., within our predicted 15–20%) under the present-day ocean circulation. However, under an inferred glacial circulation, carbonate compensation enhanced the impact of changes in nutrient utilization on atmospheric CO_2 by 32%. This stronger carbonate compensation feedback was likely due to the "focusing" of regenerated nutrients and carbon in a water mass around the CCD. In the future, we plan to expand our framework with multiple water masses, so that, for example, the impact of nutrient focusing in an isolated reservoir can be considered.

3.2. Organic Matter Burial

Our analytical framework (as well as our multibox model) predicts that the combination of organic matter burial and carbonate compensation leads to an increase in atmospheric CO_2. Although this result may seem counterintuitive, it can be understood intuitively as follows. After a mole of phosphorus has first become available for biological production, it provides for a net uptake of CO_2 from the atmosphere at two points in time: (1) the first time the mole of phosphorus is incorporated into organic matter and (2) the first time the mole of phosphorus, incorporated in organic matter, is remineralized in the deep ocean. At this point, DIC is released into the deep ocean, leading to a decrease in deep-ocean $[CO_3^{2-}]$, since $\delta[CO_3^{2-}] \approx \delta A - \delta C$. This, in turn, leads to a net dissolution of $CaCO_3$ and an ocean alkalinity increase. Once the ocean-atmosphere system has equilibrated, the alkalinity increase will have led to an uptake of CO_2 from the atmosphere into the ocean.

When the mole of phosphorus is finally buried, the CO_2 uptake achieved in step (1) is made permanent, while the step (2) CO_2 uptake is reversed. The carbonate compensation proceeds in the other direction, leading to a decrease in ocean alkalinity and an outgassing of CO_2 from the ocean into the atmosphere. This outgassing is expected to take place on the ~4–16 kyr timescales associated with the equilibration of the sediments (Lord et al., 2016), with a long tail due to the continuing equilibration and reequilibration between the ocean and the atmosphere. Thus, the impact of organic matter burial depends on the timescale that one considers. The residence time of phosphorus in the ocean is estimated to be 10–40 kyr (Filippelli, 2011; Ruttenberg, 2003), which means that uptake in step (2) and its reversal can safely be neglected on timescales of millions of years but not on timescales of tens of thousands of years.

Could this mechanism have played a role in glacial-interglacial CO_2 changes? Broecker (1982) suggested that at the end of glacial-interglacial transitions, enhanced organic matter burial may have occurred on newly flooded continental shelves. However, Peacock et al. (2006) argued that this mechanism can only be responsible for a small portion of the deglacial weakening of the soft-tissue carbon pump, based on the thickness of the deglacial sediment cover on the Sunda Shelf—the world's largest shallow shelf (Hanebuth et al., 2000). Moreover, Kohfeld and Ridgwell (2009) suggested that the deglacial sea level rise occurred too late for this mechanism to have played a major role in the deglacial rise in atmospheric CO_2. The continental shelves only flooded toward the end of the deglaciation, after the main Northern Hemisphere ice sheets had melted, and the carbonate compensation process would have taken place even later. In response to both these objections, we wish to point out that recent observations suggest that enhanced deglacial productivity may have occurred in the open ocean, rather than on newly flooded continental shelves. In fact, deglacial maxima in productivity proxies such as opal accumulation and biogenic Ba have been found at deep-sea sites in the Atlantic (Gil et al., 2009; Meckler et al., 2013; Romero et al., 2008), the Pacific (Galbraith et al., 2007; Hayes et al., 2011; Jaccard et al., 2005; Kohfeld & Chase, 2011), and the Southern Ocean (Anderson et al., 2009; Jaccard et al., 2013). Although it remains difficult to quantify from these observations the total amount of organic matter

buried, together they suggest that the deglacial decrease of the ocean nutrient inventory could have been more significant than generally recognized.

3.3. Restoring Deep-Ocean $[CO_3^{2-}]$: Preservation Versus Production

The assumption that the deep-ocean $[CO_3^{2-}]$ returns to its original value after a disturbance is key to the application of our framework. The geological record provides strong evidence for this assumption. Focusing on glacial-interglacial cycles, the B/Ca proxy indicates only small changes in the deep-ocean $[CO_3^{2-}]$ (in particular if averaged over different locations; Doss & Marchitto, 2013; Kerr et al., 2017; Raitzsch et al., 2011; Rickaby et al., 2010; Yu et al., 2010, 2014). That said, a study of 31 cores from the Pacific, Atlantic, and Indian Oceans specifically focused on $CaCO_3$ dissolution proxies (Mekik et al., 2012) did not find strong evidence for a global deglacial carbonate preservation maximum, which presents somewhat of a mystery from the conventional carbonate compensation perspective.

Perhaps, the focus has been too much on $CaCO_3$ dissolution and preservation: a large net deglacial $CaCO_3$ accumulation could also be achieved through an increase in $CaCO_3$ production. For example, a deglacial maximum in organic matter production would likely have been accompanied by a deglacial maximum in $CaCO_3$ production. Due to POC being remineralized at faster rates than $CaCO_3$, the global average $CaCO_3$:POC ratio of material collected in sediment traps at depths below ~1,000 m is close to 1:1 (Figure 4c in Archer, 1996), which implies an output of carbon and alkalinity in a ~1:1 ratio. If this ratio applied during a deglacial burial event, then the organic matter burial and the alkalinity output needed to maintain a constant whole-ocean $[CO_3^{2-}]$ would have occurred simultaneously (since $\delta[CO_3^{2-}] \approx \delta A - \delta C$). Thus, a combined burial of POC and $CaCO_3$ would have accelerated the carbonate compensation process. From this perspective, it is interesting that the deglacial oceanic productivity maximum appears to be accompanied by a maximum in the $CaCO_3$ fraction of the sediments (Brunelle et al., 2010; Flores et al., 2003; Gebhardt et al., 2008; Jaccard et al., 2005; Jaccard et al., 2013; Rickaby et al., 2010). Enhanced $CaCO_3$ production is a particularly viable explanation for deglacial $CaCO_3$ maxima at locations with continuous $CaCO_3$ accumulation, such as the Cape Basin (Flores et al., 2003) and the Weddell Sea (Rickaby et al., 2010). However, even at locations without continuous $CaCO_3$ accumulation (e.g., the deep North Pacific, Jaccard et al., 2005; and the deep Southern Ocean, Jaccard et al., 2013) where deglacial $CaCO_3$ spikes represent transient deepenings of the CCD, these CCD deepenings could ultimately be driven by $CaCO_3$ production. The CCD is the level where the supply and dissolution of $CaCO_3$ are equal. Hence, the CCD deepens when the $CaCO_3$ supply increases, even if the $CaCO_3$ dissolution rate remains constant.

4. Conclusions

We have created an analytical framework for quantifying the impacts on atmospheric CO_2 of various carbon cycle disturbances after carbonate compensation has been completed. We think that a few points are crucial:

1. Carbonate compensation amplifies by ~15–20% changes in atmospheric CO_2 resulting from redistribution of carbon within the ocean-atmosphere system (due to changes in temperature, salinity, and nutrient utilization).
2. Counterintuitively, the combination of organic matter burial in the ocean and carbonate compensation leads to an increase in atmospheric CO_2. According to our framework, changes in the soft-tissue carbon pump have very similar impacts on atmospheric CO_2 after carbonate compensation, regardless of their origin. That is, burial of 10% of the nutrient inventory has almost the same impact as a 10% decrease in the nutrient utilization.
3. The impact of carbonate compensation on atmospheric CO_2 predicted from our analytical theory is consistent with multibox model calculations involving the full set of reactions involved in the ocean-atmosphere exchange of carbon, including the boron species, H^+, and OH^-.

In the near future, we intend to apply our framework to investigate hypotheses about the glacial-interglacial CO_2 changes quantitatively. However, our framework can also be used to assess the long-term fate of anthropogenic CO_2.

Appendix A: Multibox Setup

The multibox model was modified from an earlier version used in Omta et al. (2013, 2016). The initial tracer concentrations are listed in Table A1, along with their respective values at the end of the spin-up. In Table A2, the model parameters (e.g., box volumes and transport rates) and their respective values are listed.

Table A1
Description of Multibox Model Variables, With Their Respective Meanings, Units, and Values at the End of the Spin-Up

Variables	Units	Meaning	Initial value	Value after spin-up
A_s	mol eq/m^3	Southern Ocean alkalinity	2.200	2.260
A_l	mol eq/m^3	Low-latitude alkalinity	2.200	2.227
A_n	mol eq/m^3	North Atlantic alkalinity	2.200	2.221
A_i	mol eq/m^3	NADW alkalinity	2.400	2.235
A_d	mol eq/m^3	AABW alkalinity	2.400	2.363
C_s	mol/m^3	Southern Ocean DIC concentration	2.160	2.095
C_l	mol/m^3	Low-latitude DIC concentration	2.160	1.958
C_n	mol/m^3	North Atlantic DIC	2.160	2.040
C_i	mol/m^3	NADW DIC concentration	2.350	2.249
C_d	mol/m^3	AABW DIC concentration	2.350	2.353
P_s	mol eq/m^3	Southern Ocean phosphorus concentration	5.000×10^{-5}	8.338×10^{-5}
P_l	mol eq/m^3	Low-latitude phosphorus concentration	5.000×10^{-5}	0.9059×10^{-5}
P_n	mol eq/m^3	North Atlantic phosphorus concentration	5.000×10^{-5}	4.564×10^{-5}
P_i	mol eq/m^3	NADW phosphorus	2.000×10^{-3}	1.934×10^{-3}
P_d	mM	AABW phosphorus	2.000×10^{-3}	2.068×10^{-3}
X_{CO_2}	ppmv	Atmospheric CO_2 mixing ratio	200.0	296.6

Notes. NADW = North Atlantic Deep Water; AABW = Antarctic Bottom Water; DIC = dissolved inorganic carbon.

Table A2
Description of Multibox Model Parameters (Par), With Their Respective Units, Meanings, and Values

Par	Units	Meaning	Standard value
Vol_s	m^3	Southern Ocean surface box volume	4.2×10^{16}
Vol_l	m^3	Low-latitude surface box volume	6.0×10^{16}
Vol_n	m^3	North Atlantic surface box volume	1.8×10^{16}
Vol_i	m^3	NADW box volume	6.0×10^{17}
Vol_d	m^3	AABW box volume	6.0×10^{17}
M	mol	Amount of gas in atmosphere	1.8×10^{20}
V_p	m/s	Piston velocity	5.0×10^{-5}
m_{sl}	Sv	Bidirectional mixing between Southern Ocean and low-latitude boxes	20.0
m_{lh}	Sv	Bidirectional mixing between low-latitude and North Atlantic boxes	20.0
m_{hi}	Sv	Bidirectional mixing between NADW and North Atlantic boxes	10.0
m_{id}	Sv	Bidirectional mixing between NADW and AABW boxes	2.0
m_{li}	Sv	Bidirectional mixing between NADW and low-latitude boxes	2.0
m_{si}	Sv	Bidirectional mixing between Southern Ocean and NADW boxes	5.0
q_n	Sv	NADW overturning transport	15.0
q_s	Sv	AABW overturning transport	15.0
$R_{C:P}$	–	Carbon:phosphorus ratio soft tissue	106
R_{calc}	–	Inorganic:organic carbon ratio of remineralization	0.1
T_s	°C	Southern Ocean temperature	3
T_l	°C	Low-latitude box temperature	20
T_d	°C	North Atlantic temperature	5
λ_s	s^{-1}	Southern Ocean export rate	1.07×10^{-8}
λ_l	s^{-1}	Low-latitude export rate	6.43×10^{-8}
λ_n	s^{-1}	North Atlantic export rate	2.14×10^{-8}
$[CO_3^{2-}]_{\mathrm{eq}}$	mol/m^3	Equilibrium $[CO_3^{2-}]$ in the AABW box	0.01
τ	kyr	Carbonate compensation time	5.0

Notes. NADW = North Atlantic Deep Water; AABW = Antarctic Bottom Water.

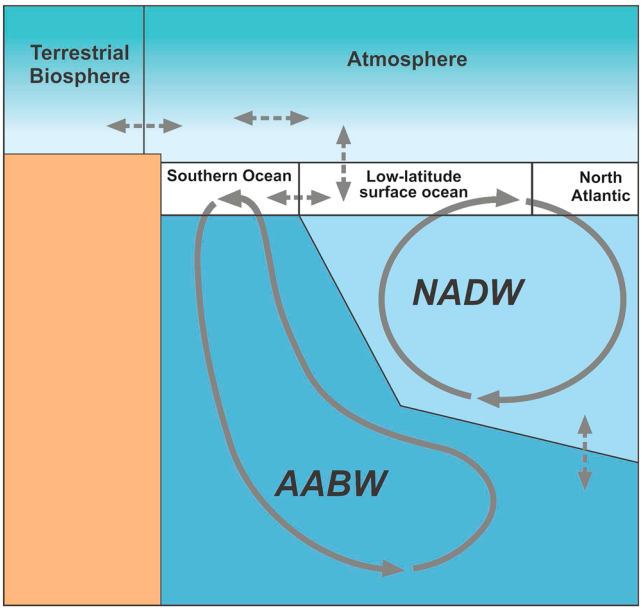

Figure A1. A schematic depiction of the multibox setup; box volumes, transport rates, and tracer concentrations before and after the spin-up are listed in Tables A1 and A2.

There are well-mixed atmospheric, low-latitude surface ocean, North Atlantic surface ocean, Southern Ocean surface, North Atlantic Deep Water (NADW), and Antarctic Bottom Water (AABW) boxes (Figure A1). A terrestrial biosphere compartment is also included in the model, but the size of this compartment is kept constant in the simulations. For the oceanic boxes, tracer concentrations are calculated through three modules: ocean-atmosphere carbon exchange, carbon isotope partitioning, and oceanic transport. For each surface ocean box, the carbon exchange module calculates the oceanic X_{CO_2} using DIC, alkalinity, and the water temperature of the box by solving the full carbonate system with the Follows et al. (2006) scheme. Then, the air-sea flux of carbon ϕ between the box and the atmosphere is calculated from the difference between $X_{CO_{2,oce}}$ and $X_{CO_{2,atm}}$:

$$\phi = V_p a k_0 (X_{CO_{2,atm}} - X_{CO_{2,oce}}) \tag{A1}$$

with V_p the piston velocity and ak_0 an equilibrium constant. Tracers are exchanged between the oceanic boxes through bidirectional mixing between boxes j and k with volumes Vol_j and Vol_k at rates m_{jk} and through overturning transports q_n (NADW) and q_s (AABW). For each tracer Y, it consists of the following equations (with the subscripts n, l, s, i, and d indicating the North Atlantic surface, low-latitude surface, Southern Ocean surface, NADW, and AABW boxes, respectively):

$$\frac{\partial Y_n}{\partial t} = \frac{-(q_n + m_{lh})(Y_n - Y_l) - m_{hi}(Y_n - Y_i)}{Vol_n} \tag{A2}$$

$$\frac{\partial Y_l}{\partial t} = \frac{-(q_n + m_{li})(Y_l - Y_i) - m_{ln}(Y_l - Y_n) - m_{ls}(Y_l - Y_s)}{Vol_l} \tag{A3}$$

$$\frac{\partial Y_s}{\partial t} = \frac{-q_s(Y_s - Y_d) - m_{si}(Y_s - Y_i) - m_{ls}(Y_s - Y_l)}{Vol_s} \tag{A4}$$

$$\frac{\partial Y_i}{\partial t} = \frac{-(q_n + m_{hi})(Y_i - Y_h) - m_{id}(Y_i - Y_d) - m_{li}(Y_i - Y_l)}{Vol_i} \tag{A5}$$

$$\frac{\partial Y_d}{\partial t} = \frac{-q_s(Y_d - Y_s) - m_{id}(Y_d - Y_i)}{Vol_d} \tag{A6}$$

We assume that dissolved inorganic phosphorus is the limiting nutrient. To represent the soft-tissue carbon pump, phosphorus is taken out of the surface boxes at rates λ_j from the surface boxes (as in Zhang et al., 2001), along with carbon through a constant Redfield ratio ($R_{C:P} = 106$). The carbonate pump is represented through a constant $CaCO_3$:POC ratio of the exported carbon ($R_{\mathrm{calc}} = 0.1$). The exported phosphorus, carbon, and alkalinity are added to the deep boxes, with one third going to the AABW box and two thirds going to the NADW box; no burial of organic matter takes place in the standard setup. Following various earlier studies (Boudreau, 2013; Boyle, 1983; Broecker & Peng, 1982; Köhler et al., 2010), the carbonate compensation feedback is formulated as a linear relaxation toward an equilibrium carbonate ion concentration ($[CO_3^{2-}]_{\mathrm{eq}}$) in the deep (AABW) box:

$$\frac{\partial C_d}{\mathrm{d}t} = -\frac{A_d - C_d - [CO_3^{2-}]_{\mathrm{eq}}}{\tau} \tag{A7}$$

$$\frac{\partial A_d}{\mathrm{d}t} = -2\frac{A_d - C_d - [CO_3^{2-}]_{\mathrm{eq}}}{\tau} \tag{A8}$$

in which $[CO_3^{2-}]_d$ is approximated as $A_d - C_d$. We choose a response time $\tau = 5$ kyr, because recent simulations with the Grid Enabled Integrated Earth system model (GENIE) have indicated that the effective carbonate compensation timescale is ~5 kyr for relatively small total carbon emissions of ~1,000 Pg (Lord et al., 2016). These emissions are of a similar order of magnitude as the amounts of carbon that are exchanged between different reservoirs before carbonate compensation in the situations under consideration (0–100 Pg in the temperature change experiments and 0–700 Pg in the carbon burial experiments).

Acknowledgments
The authors would like to thank Mick Follows, Ros Rickaby, Ed Boyle, Andy Ridgwell, and an anonymous reviewer for helpful comments and inspiring discussions. Ian Hall created the schematic of the multibox model (Figure A1). The model code and output can be accessed through https://www.dropbox.com/sh/m89mq7szcmwna8i/AADt1ACFvQJqDWu08CXQe5mOa?dl=0. AWO was supported by the Gordon and Betty Moore Foundation (grant GBMF 3778 awarded to Mick Follows) and the Simons Foundation (SCOPE award 329108, Follows). RF acknowledges NSF support through grant OCE-1536515.

References

Anderson, R. F., Ali, S., Bradtmiller, L. I., Nielsen, S. H. H., Fleisher, M. Q., Anderson, B. E., & Burckle, L. H. (2009). Wind-driven upwelling in the Southern Ocean and the deglacial rise in atmospheric CO_2. *Science*, *323*, 1443–1448.

Archer, D., Eby, M., Brovkin, V., Ridgwell, A., Cao, L., Mikolajewicz, U., et al. (2009). Atmospheric lifetime of fossil fuel carbon dioxide. *Annual Review of Earth and Planetary Science*, *37*, 117–134.

Archer, D. E. (1996). A data-driven model of the global calcite lysocline. *Global Biogeochemical Cycles*, *10*, 511–526. https://doi.org/10.1029/96GB01521

Archer, D. E. (2005). Fate of fossil fuel CO_2 in geologic time. *Journal of Geophysical Research*, *110*, C09S05. https://doi.org/10.1029/2004JC002625

Archer, D. E., & Maier-Reimer, E. (1994). Effect of deep-sea sedimentary calcite preservation on atmospheric CO_2 concentration. *Nature*, *367*, 260–264.

Archer, D. E., Kheshgi, H., & Maier-Reimer, E. (1997). Multiple timescales for neutralization of fossil fuel CO_2. *Geophysical Research Letters*, *24*, 405–408.

Archer, D. E., Kheshgi, H., & Maier-Reimer, E. (1998). Dynamics of fossil fuel CO_2 neutralization by marine $CaCO_3$. *Global Biogeochemical Cycles*, *12*, 259–276.

Archer, D. E., Eshel, G., Winguth, A., Broecker, W., Pierrehumbert, R., Tobis, M., & Jacob, R. (2000). Atmospheric pCO_2 sensitivity to the biological pump in the ocean. *Global Biogeochemical Cycles*, *14*, 1219–1230.

Bernardello, R., Marinov, I., Palter, J. B., Sarmiento, J. L., Galbraith, E. D., & Slater, R. D. (2014). Response of the ocean natural carbon storage to projected twenty-first-century climate change. *Journal of Climate*, *27*, 2033–2053.

Bolin, B., & Eriksson, E. (1959). Distribution of matter in the sea and the atmosphere. In B. Bolin (Ed.), *The atmosphere and the sea in motion*. New York: The Rockefeller Institute Press.

Boudreau, B. P. (2013). Carbonate dissolution rates at the deep ocean floor. *Geophysical Research Letters*, *40*, 744–748.

Boyle, E. A. (1983). Chemical accumulation variations under the Peru current during the past 130,000 years. *Journal of Geophysical Research*, *88*, 7667–7680.

Boyle, E. A. (1988). Vertical oceanic nutrient fractionation and glacial/interglacial CO_2 cycles. *Nature*, *331*, 55–56.

Broecker, W. S. (1982). Ocean chemistry during glacial time. *Geochimica et Cosmochimica Acta*, *46*, 1689–1705.

Broecker, W. S., & Peng, T. H. (1982). *Tracers in the Sea Lamont-Doherty Geological Observatory*. Palisades: NY.

Brovkin, V., Ganopolski, A., Archer, D. E., & Munhoven, G. (2012). Glacial CO_2 cycle as a succession of key physical and biogeochemical processes. *Climate of the Past*, *8*, 251–264.

Brunelle, B. G., Sigman, D. M., Jaccard, S. L., Keigwin, L. D., Plessen, B., Schettler, G., et al. (2010). Glacial/interglacial changes in nutrient supply and stratification in the western subarctic North Pacific since the penultimate glacial maximum. *Quaternary Science Reviews*, *29*, 2579–2590.

Chester, R. (2000). *Marine geochemistry* (2nd ed.). Oxford: Blackwell.

Chikamoto, M. O., Abe-Ouchi, A., Oka, A., Ohgaito, R., & Timmermann, A. (2012). Quantifying the ocean's role in glacial CO_2 reductions. *Climate of the Past*, *8*, 545–563.

d'Orgeville, M., England, M. H., & Sijp, W. P. (2011). Buffered versus non-buffered ocean carbon reservoir variations: Application to the sensitivity of atmospheric pCO_2 to ocean circulation changes. *Geophysical Research Letters*, *38*, L24603. https://doi.org/10.1029/2011GL049823

Doss, W., & Marchitto, T. M. (2013). Glacial deep ocean sequestration of CO_2 driven by the eastern equatorial Pacific biologic pump. *Earth and Planetary Science Letters*, *377*, 43–54.

Filippelli, G. M. (2011). Phosphate rock formation and marine phosphorus geochemistry: The deep time perspective. *Chemosphere*, *84*, 759–766.

Flores, J. A., Marino, M., Sierro, F. J., Hodell, D. A., & Charles, C. D. (2003). Calcareous plankton dissolution pattern and coccolithophore assemblages during the last 600 kyr at ODP Site 1089 (Cape Basin, South Atlantic): Paleoceanographic implications. *Palaeogeography, Palaeoclimatology, Palaeoecology*, *196*, 409–426.

Follows, M. J., Ito, T., & Dutkiewicz, S. (2006). On the solution of the carbonate system in biogeochemistry models. *Ocean Models*, *12*, 290–301.

Galbraith, E. D., Jaccard, S. L., Pedersen, T. F., Sigman, D. M., Haug, G. H., Cook, M., et al. (2007). Carbon dioxide release from the North Pacific abyss during the last deglaciation. *Nature*, *449*, 890–893.

Gebhardt, H., Sarnthein, M., Grootes, P. M., & Kiefer, T. (2008). Paleonutrient and productivity records from the subarctic North Pacific for Pleistocene glacial terminations I to V. *Paleoceanography*, *23*, PA4212. https://doi.org/10.1029/2007PA001513

Gil, I. M., Keigwin, L. D., & Abrantes, F. G. (2009). Deglacial diatom productivity and surface ocean properties over the Bermuda Rise, northeast Sargasso Sea. *Paleoceanography*, *24*, PA4101. https://doi.org/10.1029/2008PA001729

Goodwin, P., Follows, M. J., & Williams, R. G. (2008). Analytical relationships between atmospheric carbon dioxide, carbon emissions, and ocean processes. *Global Biogeochemical Cycles*, *22*, GB3030. https://doi.org/10.1029/2008GB003184

Goodwin, P., & Lenton, T. M. (2009). Quantifying the feedback between ocean heating and CO_2 solubility as an equivalent carbon emission. *Geophysical Research Letters*, *36*, L15609. https://doi.org/10.1029/2009GL039247

Goodwin, P., Oliver, K. I. C., & Lenton, T. M. (2011). Observational constraints on the causes of Holocene CO_2 change. *Global Biogeochemical Cycles*, *25*, GB3011. https://doi.org/10.1029/2010GB003888

Goodwin, P., & Ridgwell, A. (2010). Ocean-atmosphere partitioning of anthropogenic carbon dioxide on multi-millenial timescales. *Global Biogeochemical Cycles*, *24*, GB2014. https://doi.org/10.1029/2008GB003449

Goodwin, P., Williams, R. G., Follows, M. J., & Dutkiewicz, S. (2007). Ocean-atmosphere partitioning of anthropogenic carbon dioxide on centennial timescales. *Global Biogeochemical Cycles*, *21*, GB1014. https://doi.org/10.1029/2006GB002810

Goodwin, P., Williams, R. G., Ridgwell, A., & Follows, M. J. (2009). Climate sensitivity to the carbon cycle modulated by past and future changes in ocean chemistry. *Nature Geoscience*, *2*, 145–150.

Hain, M. P., Sigman, D. M., & Haug, G. H. (2010). Carbon dioxide effects of Antarctic stratification, North Atlantic Intermediate Water formation, and subantarctic nutrient drawdown during the last ice age: Diagnosis and synthesis in a geochemical box model. *Global Biogeochemical Cycles*, *24*, GB4023. https://doi.org/10.1029/2010GB003790

Hanebuth, T., Stattegger, K., & Grootes, P. (2000). Rapid flooding of the Sunda Shelf: A late-glacial sea-level record. *Science*, *288*, 1033–1035.

Hayes, C. T., Anderson, R. F., & Fleisher, M. Q. (2011). Opal accumulation rates in the equatorial Pacific and mechanisms of deglaciation. *Paleoceanography*, *26*, PA1207. https://doi.org/10.1029/2010PA002008

Ito, T., & Follows, M. J. (2005). Preformed phosphate, soft-tissue pump and atmospheric CO_2. *Journal of Marine Research*, *63*, 813–839.

Jaccard, S. L., Haug, G. H., Sigman, D. M., Pedersen, T. F., Thierstein, H. R., & Röhl, U. (2005). Glacial/interglacial changes in subarctic North Pacific stratification. *Science*, *308*, 1003–1006.

Jaccard, S. L., Hayes, C. T., Martínez-García, A., Hodell, D. A., Sigman, D. M., & Haug, G. H. (2013). Two modes of changes in Southern Ocean productivity over the past million years. *Science*, *339*, 1419–1423.

Kerr, J., Rickaby, R. E. M., Yu, J., Elderfield, H., & Sadekov, A. Y. (2017). The effect of ocean alkalinity and carbon transfer on deep-sea carbonate ion concentration during the past five glacial cycles. *Earth and Planetary Science Letters*, *471*, 42–53.

Klaas, C., & Archer, D. E. (2002). Association of sinking organic matter with various types of mineral ballast in the deep sea: Implications for the rain ratio. *Global Biogeochemical Cycles*, *16*, 1116.

Kohfeld, K. E., & Chase, Z. (2011). Controls on deglacial changes in biogenic fluxes in the North Pacific Ocean. *Quaternary Science Reviews*, *30*, 3350–3363.

Kohfeld, K. E., & Ridgwell, A. (2009). Glacial-interglacial variability in atmospheric CO_2. In C. le Quéré & E. S. Saltzman (Eds.), *Surface ocean—Lower atmosphere processes* (pp. 251–286). Washington, DC: American Geophysical Union.

Köhler, P., Fischer, H., & Schmitt, J. (2010). Atmospheric $\delta^{13}CO_2$ and its relation to pCO_2 and deep ocean $\delta^{13}C$ during the late Pleistocene. *Paleoceanography*, *25*, PA1213. https://doi.org/10.1029/2008PA001703

Kwon, E. Y., Sarmiento, J. L., Toggweiler, J. R., & de Vries, T. (2011). The control of atmospheric pCO_2 by ocean ventilation change: The effect of the oceanic storage of biogenic carbon. *Global Biogeochemical Cycles*, *25*, GB3026. https://doi.org/10.1029/2011GB004059

Lord, N. S., Ridgwell, A., Thorne, M. C., & Lunt, D. J. (2016). An impulse response function for the "long tail" of excess atmospheric CO_2 in an Earth system model. *Global Biogeochemical Cycles*, *30*, 2–17. https://doi.org/10.1002/2014GB005074

Lüthi, D., Le Floch, M., Bereiter, B., Blunier, T., Barnola, J. M., Siegenthaler, U., et al. (2008). High-resolution carbon dioxide concentration record 650,000–800,000 years before present. *Nature*, *453*, 379–382.

Marinov, I., Follows, M. J., Gnanadesikan, A., Sarmiento, J. L., & Slater, R. D. (2008). How does ocean biology affect atmospheric pCO_2? Theory and models. *Journal of Geophysical Research: Oceans*, *113*, C07032. https://doi.org/10.1029/2007JC004598

Marinov, I., Gnanadesikan, A., Sarmiento, J. L., Toggweiler, J. R., Follows, M. J., & Mignone, B. K. (2008). Impact of oceanic circulation on biological carbon storage in the ocean and atmospheric CO_2. *Global Biogeochemical Cycles*, *22*, GB3007. https://doi.org/10.1029/2007GB002958

Meckler, A. N., Sigman, D. M., Gibson, K. A., François, R., Martínez-García, A., Jaccard, S. L., et al. (2013). Deglacial pulses of deep-ocean silicate into the subtropical North Atlantic Ocean. *Nature*, *495*, 495–498.

Mekik, F. A., Anderson, R. F., Loubere, P., François, R., & Richard, M. (2012). The mystery of the missing deglacial preservation maximum. *Quaternary Science Reviews*, *39*, 60–72.

Menviel, L., Timmermann, A., Mouchet, A., & Timm, O. (2008). Climate and marine carbon cycle response to changes in the strength of the Southern Hemispheric westerlies. *Paleoceanography*, *23*, PA4201. https://doi.org/10.1029/2008PA001604

Montenegro, A., Brovkin, V., Eby, M., Archer, D., & Weaver, A. J. (2007). Long term fate of anthropogenic carbon. *Geophysical Research Letters*, *34*, L19707. https://doi.org/10.1029/2007GL030905

Omta, A. W., Bruggeman, J., Kooijman, S. A. L. M., & Dijkstra, H. A. (2006). The biological carbon pump revisited: Feedback mechanisms between climate and the Redfield ratio. *Geophysical Research Letters*, *33*, L14613. https://doi.org/10.1029/2006GL026213

Omta, A. W., Dutkiewicz, S., & Follows, M. J. (2011). Dependence of the ocean-atmosphere partitioning of carbon on temperature and alkalinity. *Global Biogeochemical Cycles*, *25*, GB1003. https://doi.org/10.1029/2010GB003839

Omta, A. W., Goodwin, P., & Follows, M. J. (2010). Multiple regimes of air-sea carbon partitioning identified from constant-alkalinity buffer factors. *Global Biogeochemical Cycles*, *24*, GB3008. https://doi.org/10.1029/2009GB003726

Omta, A. W., Kooi, B. W., van Voorn, G. A. K., Rickaby, R. E. M., & Follows, M. J. (2016). Inherent characteristics of sawtooth cycles can explain different glacial periodicities. *Climate Dynamics*, *46*, 557–569.

Omta, A. W., van Voorn, G. A. K., Rickaby, R. E. M., & Follows, M. J. (2013). On the potential role of marine calcifiers in glacial-interglacial dynamics. *Global Biogeochemical Cycles*, *27*, 692–704. https://doi.org/10.1002/gbc.20060

Oschlies, A., Riebesell, K. G. S. U., & Schmittner, A. (2008). Simulated 21st century's increase in oceanic suboxia by CO_2-enhanced biotic carbon export. *Global Biogeochemical Cycles*, *22*, GB4008. https://doi.org/10.1029/2007GB003147
Peacock, S., Lane, E., & Restrepo, J. M. (2006). A possible sequence of events for the generalized glacial-interglacial cycle. *Global Biogeochemical Cycles*, *20*, GB2010. https://doi.org/10.1029/2005GB002448
Petit, J. R., Jouzel, J., Raynaud, D., Barkov, N. I., Barnola, J.-M., Basile, I., et al. (1999). Climate and atmospheric history of the past 420,000 years from the Vostok ice core, Antarctica. *Nature*, *399*, 429–436.
Pytkowicz, R. M., & Conners, D. N. (1964). High pressure solubility of calcium carbonate in seawater. *Science*, *144*, 840–841.
Raitzsch, M., Hathorne, E. C., Kuhnert, H., Groeneveld, J., & Bickert, T. (2011). Modern and late Pleistocene B/Ca ratios of the benthic foraminifer Planulina wuellerstorfi determined with laser ablation ICP-MS. *Geology*, *39*, 1039–1042.
Rickaby, R. E. M., Elderfield, H., Roberts, N. L., Hillenbrand, C. D., & Mackensen, A. (2010). Evidence for elevated alkalinity in the glacial Southern Ocean. *Paleoceanography*, *25*, PA1209. https://doi.org/10.1029/2009PA001762
Ridgwell, A., & Hargreaves, J. C. (2007). Regulation of atmospheric CO_2 by deep-sea sediments in an Earth system model. *Global Biogeochemical Cycles*, *21*, GB2008. https://doi.org/10.1029/2006GB002764
Ridgwell, A., & Zeebe, R. E. (2005). The role of the global carbonate cycle in the regulation and evolution of the Earth system. *Biogeosciences*, *234*, 299–315.
Riebesell, U., Schulz, K. G., Bellerby, R. G., Botros, M., Fritsche, P., Meyerhöfer, M., et al. (2007). Enhanced biological carbon consumption in a high CO_2 ocean. *Nature*, *450*, 544–548.
Romero, O. E., Kim, J. H., & Donner, B. (2008). Submillennial-to-millennial variability of diatom production off Mauretania, NW Africa, during the last glacial cycle. *Paleoceanography*, *23*, PA3218. https://doi.org/10.1029/2008PA001601
Ruttenberg, K. C. (2003). The global phosphorus cycle. In D. M. Karl & W. H. Schlesinger (Eds.), *Treatise on geochemistry, biogeochemistry* (Vol. 8, pp. 585–643). San Diego, CA: Elsevier.
Sarmiento, J. L., & Gruber, N. (2006). *Ocean biogeochemical dynamics*. Princeton, NJ: Princeton University Press.
Sigman, D. M., & Boyle, E. A. (2000). Glacial-interglacial variations in atmospheric carbon dioxide. *Nature*, *407*, 859–869.
Sigman, D. M., McCorkle, D. C., & Martin, W. R. (1998). The calcite lysocline as a constraint on glacial/interglacial low-latitude production changes. *Global Biogeochemical Cycles*, *3*, 409–427.
Sigman, D. M., Hain, M. P., & Haug, G. H. (2010). The polar ocean and glacial cycles in atmospheric CO_2 concentration. *Nature*, *466*, 47–55.
Volk, T., & Hoffert, M. I. (1985). Ocean carbon pumps: Analysis of relative strengths and efficiencies in ocean-driven atmospheric CO_2. In E. T. Sundquist & W. S. Broecker (Eds.), *The carbon cycle and atmospheric CO_2: Natural variations Archean to Present* (pp. 99–110). Washington DC: American Geophysical Union.
Wallmann, K. (2014). Is late Quaternary climate change governed by self-sustained oscillations in atmospheric CO_2? *Geochimica et Cosmochimica Acta*, *132*, 413–439.
Williams, R. G., & Follows, M. J. (2011). *Ocean dynamics and the carbon cycle*. Cambridge: Cambridge University Press.
Yamanaka, Y., & Tajika, E. (1996). The role of the vertical fluxes of particulate organic matter and calcite in the oceanic carbon cycle: Studies using an ocean biogeochemical general circulation model. *Global Biogeochemical Cycles*, *10*, 361–382.
Yu, J., Broecker, W. S., Elderfield, H., Jin, Z., McManus, J., & Zhang, F. (2010). Loss of carbon from the deep sea since the Last Glacial Maximum. *Science*, *330*, 1084–1087.
Yu, J., Anderson, R., Jin, Z. D., Menviel, L., Zhang, F., Ryerson, F. J., & Röhling, E. J. (2014). Deep South Atlantic carbonate chemistry and increased interocean deep water exchange during last deglaciation. *Quaternary Science Reviews*, *90*, 80–89.
Zhang, R., Follows, M. J., Grotzinger, J. P., & Marshall, J. (2001). Could the Late Permian deep ocean have been anoxic? *Paleoceanography*, *16*, 317–329.